Journal of Radiation Research, 2013, 54, 962–970
doi: 10.1093/jrr/rrt024 Advance Access Publication 19 April 2013

Effective and organ doses using helical 4DCT for thoracic and abdominal therapies

Yuka MATSUZAKI, Keisuke FUJII, Motoki KUMAGAI, Ichiro TSURUOKA and Shinichiro MORI*

Research Center for Charged Particle Therapy, National Institute of Radiological Sciences, 4-9-1, Anagawa, Inage-ku, Chiba, 263-8555, Japan
*Corresponding author. Tel: +81-43-251-2111; Fax: +81-43-284-0198; Email: shinshin@nirs.go.jp

(Received 18 July 2012; revised 23 February 2013; accepted 28 February 2013)

The capacity of 4DCT to quantify organ motion is beyond conventional 3DCT capability. Local control could be improved. However we are unaware of any reports of organ dose measurements for helical 4DCT imaging. We therefore quantified the radiation doses for helical 4DCT imaging. Organ and tissue dose was measured for thoracic and abdominal 4DCT in helical mode using an adult anthropomorphic phantom. Radiation doses were measured with thermoluminescence dosimeter chips inserted at various anatomical sites on the phantom. For the helical thoracic 4DCT, organ doses were 57.2 mGy for the lung, 76.7 mGy for the thyroids, 48.1 mGy for the breasts, and 10.86 mGy for the colon. The effective doses for male and female phantoms were very similar, with a mean value of 33.1 mSv. For abdominal 4DCT imaging, organ doses were 14.4 mGy for the lung, 0.78 mGy for the thyroids, 9.83 mGy for breasts, and 58.2 mGy for the colon (all obtained by using ICRP 103). We quantified the radiation exposure for thoracic and abdominal helical 4DCT. The doses for helical 4DCT were approximately 1.5 times higher than those for cine 4DCT, however the stepwise image artifact was reduced. 4DCT imaging should be performed with care in order to minimize radiation exposure, but the advantages of 4DCT imaging mandates its incorporation into routine treatment protocols.

Keywords: radiation dose; 4DCT; helical; cine; effective dose

INTRODUCTION

Advanced treatment delivery methods, combined with state-of-the-art imaging, has, in recent years, dramatically increased target conformity. This progress though goes hand in hand with higher technical complexity. As a result, current radiotherapy as well as particle therapy can provide high doses to the target while offering optimal sparing of the surrounding healthy tissue. Dose variation due to intrafractional (respiratory/cardiac motions etc.) and interfractional (tumor shrinkage, patient setup error etc.) changes, however, may reduce treatment accuracy, particularly in the thoracic and abdominal regions. Hence the ongoing development of radiotherapy requires careful consideration of these changes [1].

Four-dimensional CT (4DCT) and serial CT scans allow us to quantify these changes and the results can be incorporated into the dose calculation to obtain improved treatment planning [2]. Hence these 4DCT scan methods are a key component for improving the accuracy of radiotherapy treatment. However, the ability of 4DCT to acquire CT images as a function of the respiratory phase comes at the cost of higher radiation doses than using conventional imaging; indeed, we previously reported that radiation doses in 4DCT in step were four times higher than those with conventional CT [3]. That study was performed using the 4DCT cine mode [4]. Others have reported the radiation dose for helical 4DCT using the Monte Carlo simulation code [5]. We are, however, unaware of any report measuring radiation doses (organ dose and effective dose) for helical 4DCT imaging [6], despite the importance of this information to the incorporation of helical 4DCT into routine use. While computed tomography dose index (CTDI) phantoms are generally used for quality assurance and control purposes of the CT scanners, this method does not directly show organ or effective doses. The unanswered question of the suitability of helical 4DCT dose in radiotherapy thus remains of strong clinical interest.

Here, we quantified radiation exposure from helical 4DCT for thoracic and abdominal protocols using an anthropomorphic phantom.

MATERIALS AND METHODS

Phantom

The adult anthropomorphic phantom used for organ and tissue dose measurement consisted of 35 sections of 2.5-cm thickness modeling a human body with a height of 164 cm and a weight of 54 kg (Kyoto Kagaku Co., Japan) (Fig. 1). Assuming that the phantom consisted of elliptic cylinders and elliptic cones we estimated its total surface area to be about 1.5 m^2. Each section contained several holes (2 mm diameter and 17 mm length) for the insertion of thermoluminescence dosimeters (TLDs). The TLD insertion holes were positioned to match various relevant organs and tissues [7]. The phantom components, equivalent in density to the human body, were composed of soft tissue (1.01 g/cm^3, 3.25×10^{23} e^-/g), lung (0.3 g/cm^3, 3.31×10^{23} e^-/g) and bone (1.24 g/cm^3, 3.21×10^{23} e^-/g) [8, 9].

Data acquisition

Commercially available multi-slice CT apparatus offer cine and helical 4DCT scan mode. Cine 4DCT acquires the CT data over one respiratory cycle and then moves the CT couch to the adjacent position to obtain the next CT data within the next respiratory cycle. This process is repeated until the entire scan range is imaged and after that the reconstructed CT images are sorted into specific respiratory phases. In contrast, helical 4DCT continuously moves the CT couch with a low helical pitch. Re-sorting of helical 4DCT data uses the respiratory signal to sort the temporal scans in sinogram space, and is therefore more difficult compared to the cine mode.

Thoracic and abdominal 4DCT scans were acquired using a 16 multi-slice CT scanner (MSCT) (Aquilion LB, Toshiba Medical Systems, Japan) after scanography for patient positional verification. In helical mode this 4DCT scanner re-sorts the temporal scans in sinogram space before reconstruction using the respiratory signal. In clinical practice, a respiratory-sensing monitor acquires the respiratory signal. However since our phantom does not simulate respiratory motion and a respiratory signal is required for the image reconstruction, we have chosen an artificial 3.3-s respiratory cycle. The 4DCT scan conditions for both thoracic and abdominal regions were 120 kV, 100 mA, 0.5-s rotation time and the pitch factor $p = 0.125$ which is defined as the following:

$$p = \Delta d / T$$

where Δd = table feed (mm)/rotation (s) and T = beam width (mm). All CT scan parameters are listened in Table 1.

The pitch factor was defined on the CT console based on the respiratory cycle to acquire images at the respective patient positions. The pitch factor was optimized for a respiratory cycle of 3.3 s as shown in Fig. 2. No tube current modulation to improve image quality (auto exposure control systems: AECs) was adopted for either the craniocaudal or angular direction because the AEC cannot be selected in the 4D mode. The CT effective energies used

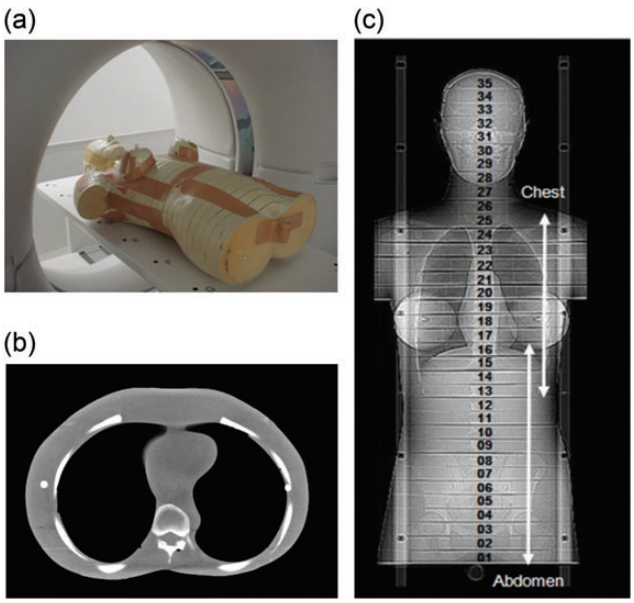

Fig. 1. Dose measurement geometry. (**a**) The anthropomorphic phantom was set on the CT bed for radiotherapy. (**b**) Axial image of the anthropomorphic phantom. (**c**) Scan regions for chest and abdominal experiments were overlaid on the scano.

Table 1. Scan conditions for helical 4D chest/abdominal CT scans

Scan conditions for scano	**Chest**	**Abdomen**
Tube voltage [kV]	120	120
Tube current [mA]	50	50
Rotation time [s]	0.5	0.5
Scan range [mm] (phantomsection no.)	500 (12–31)	525 (1–21)
Scan conditions for 4DCT	**Chest**	**Abdomen**
Tube voltage [kV]	120	120
Tube current [mA]	100	100
Rotation time [s]	0.5	0.5
Total scan time [s]	85.5	100
Slice collimation [mm]	16 × 1.0	16 × 1.0
Pitch factor	0.125	0.125
Scan FOV [mm]	400	400
Scan range [mm] (phantomsection no.)	325 (13–25)	400 (1–16)

FOV = field of view.

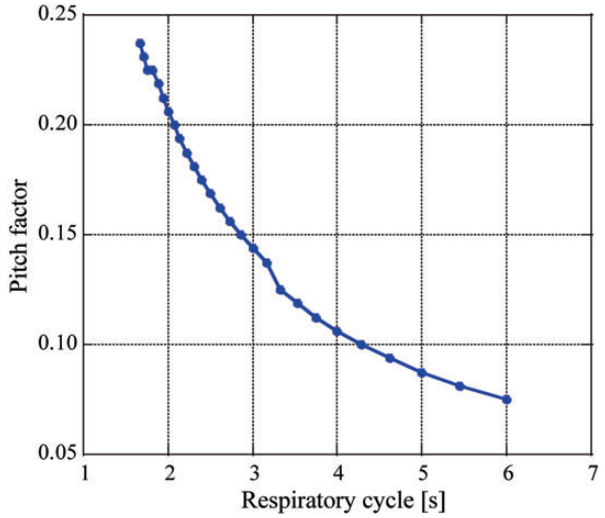

Fig. 2. Relationship between respiratory cycle and pitch factor for helical 4DCT on an Aquilion LB as obtained from the CT console. A pitch factor of 0.125 was used for a respiratory cycle of 3.3 s.

varied between 56 and 75 keV, as in our previous report [3].

Dosimetry

Organ and tissue doses in the phantoms were measured using two kinds of glass encapsulated TLDs based on their sensitivity. The sensitivity of the first TLD, UD-170A (BeO, 2 mm diameter, 8 mm length, effective atomic number 7.6; Panasonic Co. Ltd, Osaka, Japan) remains almost constant over the entire energy range used, whereas that of the second one, UD-110S ($CaSO_4$:Tm, 2 mm diameter, 10 mm length, effective atomic number 14.4; Panasonic Co. Ltd) is one order of magnitude higher than the first in the lower X-ray energy range below 50 keV. The UD-170A is therefore appropriate for dose measurement within the region directly irradiated by the X-ray beam (thoracic and abdominal regions) while the UD-110S is better suited to the measurements outside this region receiving scattered radiation. Therefore the lower sensitivity TLDs (UD-170A) were inserted in the anthropomorphic phantom within the CT scan region plus 3–4 phantom sections in both superior and inferior directions. In the other phantom sections, the low energy high sensitivity TLDs (UD-110S) were inserted.

The calibration of each TLD in the phantom was determined with two types of ionization chamber (C-110s and AE132a) exposure meter (Applied Engineering Inc., Tokyo, Japan) traceable to the Japanese National Standard at the Electrotechnical Laboratory (AIST) in Tsukuba, Japan. Two sizes of the C-110 were use, a small one (length = 22.0 mm, diameter = 6.0 mm, volume = 0.6 ml) and a larger one (length = 39.5 mm, diameter = 19.0 mm, volume = 12 ml). The UD-170A was calibrated using the small ionization chamber only, whereas the UD-110S was calibrated using both the small and the larger C-110.

The UD-170A TLDs were dedicated to measuring the depth dose and hence placed at a depth of 12.5 cm in a water equivalent slab phantom (30 cm × 30 cm × 25 cm thickness) illustrated in Fig. 3a. The smaller ionization chamber (0.6 ml) was placed into the same position. In contrast the UD-110S TLDs dedicated to measuring the scattered radiation, and the larger ionization chamber (12 ml), were set at a 10 cm lateral distance from the phantom. Further UD-170A TLDs to measure the surface dose and the ionization chamber were placed on the water equivalent slab phantom (30 cm × 30 cm × 20 cm thickness) as illustrated in Fig. 3b. The TLDs were calibrated with variable effective X-ray energies (48.1 keV (at 90 kV and 100 mAs), 62.5 keV (at 130 kV and 100 mAs) and 75.7 keV (at 140 kV and 100 mAs)) by using the kV-X-ray system, MG225 (YXLON International X-Ray GmbH, Hamburg, Germany). The effective energy range already equaled that of CT. The distance between the X-ray focus and the chamber was set to 100 cm for all calibrations. The X-ray irradiation field was 10 cm × 10 cm. All TLDs were annealed before the experiment. Approximately 200 TLDs were inserted into the respective organs and tissues and these positions were determined from radiography and fluoroscopic images of the anthropomorphic phantom [7]. The two types of TLDs in our measurements had a sensitivity variation of 7%, however, it is useful to measure dose in multiple positions at the same time. The dose measurements from the TLDs were evaluated using a commercial analyzer (UD-5160P, Panasonic Co., Japan) 48 h after the experiment. Because the large number of TLDs inserted into each organ at different positions resulted in large variation within and among organs (for example in the upper/lower lung and abdominal regions), we decided to calculate standard deviations for the location statistics rather than measurement reproducibility.

The dose to the various organs was calculated by multiplying the measured dose values from the TLDs by the appropriate correction factors. In order to compare our findings with our previous work [3] we used the tissue weighting factors (W_T) listed in the ICRP 60 and ICRP 103 [10, 11], in Table 2.

The effective doses (E) were calculated according to the ICRP 103 using the following expression:

$$E = \sum_T W_T \cdot H_T = \sum_T W_T \sum_R W_R \cdot D_{T,R} \qquad (1)$$

where H_T is the equivalent dose of the organ or tissue, the radiation weighting factor W_R is 1 because an X-ray beam was used, and D is the mean absorbed dose.

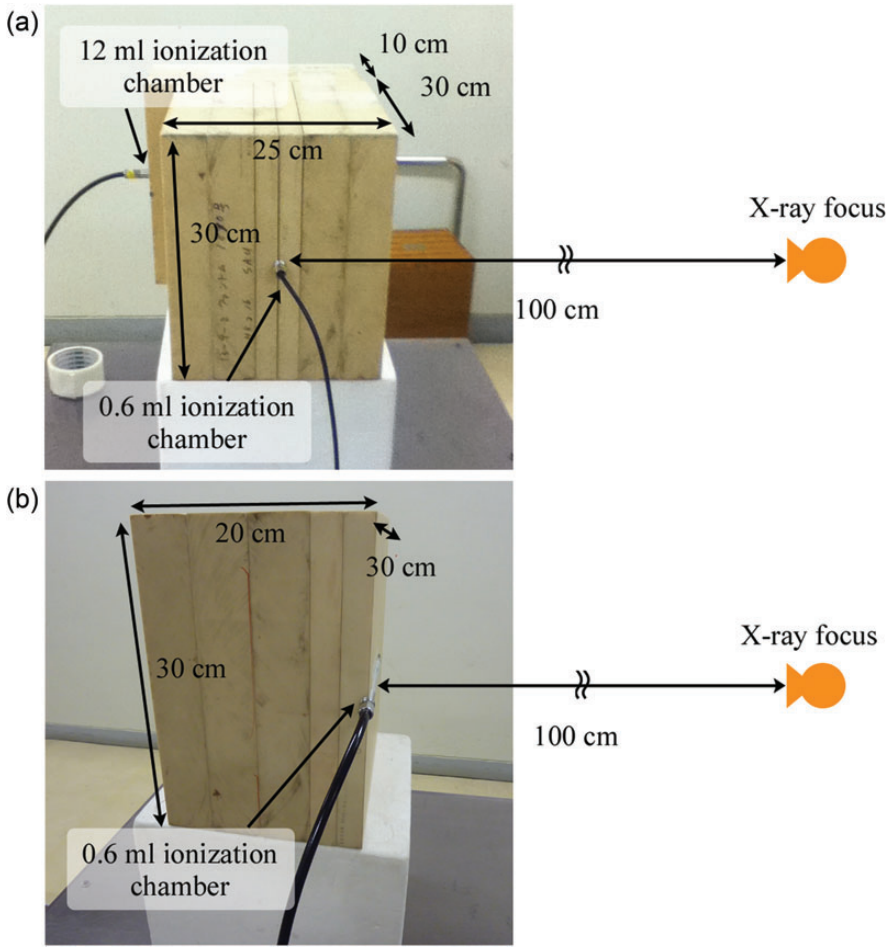

Fig. 3. (**a**) Geometry of the calibration for TLDs to measure the depth dose and dose by scattered radiation. Water equivalent slab phantom size is 30 cm × 30 cm × 25 cm thickness. The distance between X-ray focus and ionization chamber was 100 cm. (**b**) Geometry of the calibration for TLDs to measure the surface dose. Water equivalent slab phantom size is 30 cm × 30 cm × 20 cm thickness. The distance between X-ray focus and ionization chamber was 100 cm.

The absorbed dose was calculated for various organs. In the case of breast, four TLDs were inserted symmetrically around the glandular tissue in the respective breasts. The mean absorbed dose was calculated using the following formula:

$$D_{breast} = D_{soft\_tissue}(\mu_{en}/\rho)_{breast}/(\mu_{en}/\rho)_{soft\_tissue} \quad (2)$$

where D_{soft_tissue} is the dose absorbed by the soft tissue, which is equal to the mean absorbed dose D at the respective anatomical phantom position, and $(\mu_{en}/\rho)_{breast}$ and $(\mu_{en}/\rho)_{soft\_tissue}$ are the mean mass energy absorption coefficients for breast and soft tissue, respectively [12].

The absorbed dose to the colon (D_{colon}) is defined in the ICRP 67 [13], where it is represented as the sum of the partial absorbed doses. D_{ULI} is the mean absorbed dose of the large intestine in the upper colon, which consists of the ascending colon and transverse colon. D_{LLI} is the mean absorbed dose of the large intestine in the lower colon, which consists of the descending colon, the sigmoid colon and the rectum [14]. From ICRP 67 we used the following formula to calculate the dose to the colon:

$$D_{colon} = 0.57D_{ULI} + 0.43D_{LLI} \quad (3)$$

However, in the colon region as defined by ICRP 60 only the lower large intestine is contained, the upper large intestine is contained in the remaining tissues. Thus, the equation given above could not be applied to calculate the absorbed dose to the colon when using ICRP 60.

Table 2. Tissue weighting factor, W_T according to ICRP 103 and 60, respectively

Tissue weighting factor, w_T	ICRP 103	ICRP 60
Bone surface	0.01	0.01
Skin	0.01	0.01
Bladder	0.04	0.05
Oesophagus	0.04	0.05
Thyroid	0.04	0.05
Liver	0.04	0.05
Breast	0.12	0.05
Colon	0.12 (ULI + LLI)	0.12 (LLI)
Lungs	0.12	0.12
Bone marrow	0.12	0.12
Stomach	0.12	0.12
Gonads	0.08	0.20
Salivary glands	0.01	N/A
Brain	0.01	within Remainder
Remainder	0.12	0.05
Total	1.00	1.00

Remainder tissues: ICRP 103: adrenals, kidneys, muscle, pancreas, small intestine (SI), spleen, thymus, uterus/cervix, extrathoracic tissue, gall bladder, heart, lymphatic nodes, oralmucosa, prostate. ICRP 60: adrenals, kidneys, muscle, pancreas, small intestine (SI), spleen, thymus, uterus/cervix, brain, upper large intestine, N/A = not available.

Red bone marrow (D_{bone_marrow}) and bone surface ($D_{bone\_surface}$) are calculated using the following equations:

$$D_{bone\_marrow} = \sum_i D_{soft\_tissue,marrow,i} \cdot M_i \quad (4)$$

$$D_{bone\_surfacet} = \sum_i D_{soft\_tissue,bone,i} \cdot B_i \quad (5)$$

where M and B are the ratios of red bone marrow and mineralized tissue at the i-th TLD position for bone measurement, respectively [15].

To measure the surface dose, five TLDs were placed on the surface of each side (anterior, posterior, left and right) of the slice situated in the middle of the scan region. The skin dose was calculated by averaging these four parts (the sum of 20 TLDs in $1\,cm^2 \times 4$ positions). The phantom portions of the breasts and testis are removable; however, we measured organ doses for both. Each series of scano and scan was repeated twice to reduce statistical fluctuation, and the calculated result was the average of two irradiations.

RESULTS

For the thoracic 4DCT, measured organ doses were 57.2 mGy for the lung, 76.7 mGy for the thyroid, 48.1 mGy for the breasts and 10.86 mGy/6.98 mGy (ICRP 103/ICRP 60) for the colon. These values were higher than those for head and abdominal regions as the thorax was the location of CT exposure. Effective doses for male and female were very similar, 33.2 mSv/32.9 mSv (male/female, ICRP 103), 28.8 mSv/28.7 mSv (male/female, ICRP 60), with mean values of 33.1 mSv/28.8 mSv (ICRP 103/ICRP 60).

For the abdominal 4DCT, organ doses were 14.4 mGy for the lung, 0.78 mGy for the thyroids, 9.83 mGy for the breasts, and 58.2 mGy/53.8 mGy for the colon (ICRP 103/ICRP 60). Values for lung and breasts were approximately four and five times lower when using abdominal rather than thoracic 4DCT imaging. The dose to the colon was then accordingly eight-fold/five-fold higher (ICRP 60/ICRP 103). The absorbed doses for the gonad for abdominal 4DCT imaging were measured as 12.6 mGy/42.3 mGy (male/female). This is 120 and 90 times higher than those for a thoracic 4DCT. Effective doses for male and female for the abdominal 4DCT showed a similar tendency to those for the thoracic 4DCT, but the dose for female was slightly increased. Namely 29.3 mSv/31.8 mSv (male/female, ICRP 103) and 29.0 mSv/34.9 mSv (male/female, ICRP 60) with mean values of 30.5 mSv/32.0 mSv (ICRP 103/ICRP 60). The dose to the eye lens in abdominal 4DCT (0.12 mGy) was lower than that for thoracic 4DCT (1.07 mGy), while the average skin doses for the two CT scan types were almost the same (57.7 mGy for thoracic and 56.0 mGy for abdomenal 4DCT). All organ/tissue doses and effective doses are listed in Table 3.

DISCUSSION

This study quantified effective and organ doses in helical 4DCT scans with a 16 MSCT scanner and an anthropomorphic phantom. Effective doses (ICRP 103/ICRP 60) for thoracic and abdominal scans were 33.1 mSv/28.8 mSv and 30.5 mSv/32.0 mSv, respectively. These are similar to or slightly higher than those obtained with an ECG (electrocardiograph)-gated cardiac CT [16] and a multiphase contrast-enhanced CT [17–19], however they depend on the tube current value. When using ICRP 103 the effective dose of a thoracic helical scan is about 8% higher than for an abdominal scan, but when applying ICRP 60 the effective dose of the thoracic scan is about 11% lower than for an abdominal scan. This can be explained as follows. In ICRP 60, the organs in the abdominal region (e.g. gonads, stomach and colon) have been assigned higher tissue

Table 3. Results for organ and effective doses for 4DCT

	Chest		Abdomen		Ratio
Organ (Number of TLD)	**Average**	**SD**	**Average**	**SD**	**(Abdomen/Chest)**
Absorbed dose [mGy]					
Brain (8)	1.41	0.70	0.12	0.05	0.08
Salivary gland (7)	3.86	0.65	0.27	0.07	0.07
Thyroid (3)	76.7	7.3	0.78	0.11	0.01
Esophagus (3)	50.5	4.1	3.64	2.68	0.07
Lung (14)	57.2	7.5	14.4	17.1	0.25
Breast (8)	48.1	5.6	9.83	8.17	0.20
Liver (5)	48.2	7.0	51.5	3.3	1.07
Stomach (4)	48.2	4.2	57.0	2.3	1.18
Colon:ICRU 103 (10)	10.86	7.42 (D_{ULI})/4.11 (D_{LLI})	58.2	4.9 (D_{ULI})/2.8 (D_{LLI})	5.36
Colon:D_{LLI}, ICRU 60 (5)	6.98	9.55	53.8	6.4	7.70
Bladder (2)	0.36	0.10	51.9	7.0	144.07
Gonad male (3)	0.10	0.00	12.6	1.5	120.24
Gonad female (6)	0.47	0.03	42.3	6.2	90.26
Bone surface (54)	50.8	1.1	71.6	2.5	1.41
Active red bone marrow (54)	16.9	0.4	23.0	0.6	1.36
Skin (20)	12.3	1.4	14.2	2.5	1.16
Remainders					
ICRU 103					
Male (55)	31.3	20.5	29.8	23.6	0.95
Female (57)	28.2	21.7	31.3	22.7	1.11
ICRU 60					
Male (35)	28.8	19.3	38.5	23.6	1.34
Female (33)	25.8	20.2	39.2	22.2	1.52
Effective dose [mSv]					
ICRU 103					
Male	33.2		29.3		0.88
Female	32.9		31.8		0.97
Average	33.1	0.2	30.5	1.8	0.92
ICRU 60					
Male	28.8		29.0		1.01
Female	28.7		34.9		1.22
Average	28.8	0.1	32.0	4.2	1.11
Eye lens [mGy] (4)	1.07	0.10	0.12	0.01	0.11
Average skin [mGy] (20)	57.7	6.8	56.0	9.7	0.97

s.d. = standard deviation, D_{ULI} and D_{LLI} = absorbed doses of the upper and lower part of the large intestines, respectively. The number shown in parentheses is the number of TLDs inserted into every organ and tissue.

weighting factors. Contrary to this, in ICRP 103 the organs in the thoracic region (e.g. lung and breast) have been assigned higher tissue weighting factors. The tissue weighting factors for breast are higher in ICRP 103 than in ICRP 60. On the other hand, the weighting factors for gonads in ICRP 60 are higher than those in ICRP 103. Using ICRP 60 the contribution of the gonads to the effective dose was the largest share. Thus, in our measurements, the contribution of the gonad for the female phantom drove up the mean effective dose in accordance with ICRP 60. In contrast, absorbed doses from thoracic 4DCT include low radiation to the eye lens and the thyroid due to scatter radiation, whereas these organ doses are minimized with abdominal 4DCT. In our hospital, we have not yet defined the 4DCT scanning conditions, except for the tube voltage which is 120kV, however, our results can be applied to any scan conditions normalized by the tube current.

Comparison of cine and helical 4DCT

We previously reported [3] that the effective dose in thoracic cine 4DCT using a 16 multi-slice CT (LightSpeed 16-slice QX/i, General Electric Company, Wauksha, WI, USA) under scan conditions very similar to those of the present study (120 kV, 120 mA, 4 s scan time/position, 0.8 s/rotation, slice collimation of 16 × 1.25 mm) was 24.7 mSv (ICRP 60). Since the respiratory cycle was set to 3.2 s, a scan time/position of 4 s (3.2 s + one rotation (= 0.8 s)) was necessary. Given that the effective dose in this previous study was calculated using the ICRP 60, we obtained an effective dose for the helical CT for ICRP 60 of 28.8 mSv compared to 33.1 mSv when using ICRP 103. The effective dose in this study was slightly higher than that in our previous study in the cine 4DCT, even though the effective mAs value in our previous study (480 mAs) was higher than that in this study (400 mAs).

While cine 4DCT is designed for a standard bore size, helical 4DCT is designed for a larger size. The source-to-detector distances (SIDs) are approximately 950 mm for cine 4DCT and 1280 mm for helical 4DCT. The tube currents are, therefore, higher in a large bore size CT than in a standard CT. This makes it difficult to compare the two CTs, including their CT geometry because the effective dose strongly depends on the tube current value, and further on system components such as geometry and scan conditions. Given the relationship that exists between image qualities (e.g. image noise, spatial resolution and slice thickness) and dose, the radiation exposure for the different CTs should be compared at the same image quality. The helical 4DCT used in the present study is a large bore system, and accordingly requires a higher tube current to obtain the same image quality as a standard sized system. Also the slice thickness in the CT systems (helical 4DCT in this study and cine 4DCT in our previous study) is different. We therefore compared the different CTs using the quality factor Q [20], which remains constant if the phantom and X-ray effective energies are the same. $Q = D \cdot \sigma^2 \cdot \rho^3 \cdot z = const.$, where D is effective dose, σ is the magnitude of the image noise, ρ is the spatial resolution and z is slice thickness. The two kinds of phantom were used to acquire CT images using two different CTs (Toshiba Medical Systems and GE Health Care) with the same scan conditions for the respective CT scan modes. To evaluate image noise, a cylindrical water phantom (240 mm diameter) was used, and the standard deviation of the CT number in the 100-mm diameter region of interest positioned at the center of the phantom was calculated. For the spatial resolution, the PSF (point spread function) was evaluated by using a CATPHAN (module CTP528, Phantom Laboratory, Salem, NY) on an implanted 0.28 mm diameter bead.

While the reconstruction was done using a half-reconstruction algorithm with the standard kernel for both CTs, the slice thickness varied, being 1.25 mm for the cine 4DCT and 1.0 mm for the helical 4DCT. The quality factors for cine 4DCT and helical 4DCT were $Q_{cine} = 27\,148.5$ (= 24.7 mSv × (1.24 mm)^3 × (21.5 HU)^2 × 1.25 mm) and $Q_{helical} = 47\,895.9$ (= 28.8 mSv × (0.99 mm)^3 × (41.4 HU)^2 × 1.00 mm). The image noise in the scan of the water phantom is convertible into that of 4DCT knowing that the image noise varies inversely as the square root of the tube current. An effective dose of 43.5 mSv (= $Q_{helical}/\rho^3_{cine}/\sigma^2_{cine}/h_{cine}$) was necessary to obtain the same image quality in the helical 4DCT, indicating that the helical 4DCT doses need to be approximately 1.5-fold higher (= 43.5 mSv/28.8 mSv) than those for the cine 4DCT.

Dose reduction

CT manufacturers have attempted to reduce the radiation dosage from CT scans by adapting image-processing and modulated X-ray output during scanning. Examples of the former include iterative reconstruction algorithms [21], while the latter include AECs, which aim to avoid over/underdosing and to improve image quality by modulating the X-ray tube current. Moreover, the X-ray tube current is changed as a function of the cardiac phase in cardiac CT imaging. These devices (AECs and phase modulation) are not presently integrated into the Toshiba 4DCT equipment, but doing so would markedly reduce radiation doses for helical 4DCT.

In several treatment centers treatment planning for thoracic and abdominal regions is based on respiratory-gated CT images, and generally the images are recorded during the exhalation phase. Toshiba's CTs, however, generate respiratory-gated scans in helical mode only, and any radiation dose delivered outside of exhalation might accordingly be unnecessary. The above dose-reduction mechanisms have the potential to significantly reduce radiation doses by increasing the tube current values at exhalation only.

Further, it has to be considered that the radiation dosages depend on patient characteristics such as height, weight, age, etc.

The all-over dose given to a patient's tumor by the actual radiation treatment is generally in the range of 40–70 Gy for thoracic treatments [22]. This is significantly larger than that of a 4DCT acquisition for treatment planning (approximately several tens of mGy in the lung), notwithstanding the medical staff should make an effort to minimize radiation exposure with 4DCT scans as much as possible. For example, 4DCT rescans should be avoided to minimize the all-over patient dose. The main reasons for doing a rescan are degraded image quality due to unsuitable scan conditions or patient irregular breathing patterns. These factors, however, could be avoided by employing a 4DCT QA/QC protocol, and also by controlling the respiration of a patient for example using a respiratory coaching technique.

Study limitation

One limitation of this study warrants mention. The anthropomorphic phantom we used here cannot simulate respiratory motion. However, the CT radiation doses are given for a single respiratory cycle at respective CT slice positions to obtain 4D volumetric CT data. Therefore, significant CT radiation dose differences with or without a respiratory motion could not be seen.

CONCLUSION

We quantified the radiation exposure for helical 4DCT using an anthropomorphic phantom and compared results with those for a cine 4DCT. To obtain a similar noise level with these two CT modes, helical 4DCT requires ~ 1.5 times more dosage than cine 4DCT. This increase, though, is well balanced by the reduction of the stepwise image artifacts observed in the cine mode. Although the medical staff (oncologists, medical physicists, dosimetrists etc.) should continue their efforts to minimize radiation exposure during 4DCT scans, the clearly greater clinical gains provided by 4DCT mandate its incorporation into routine treatment protocols.

ACKNOWLEDGEMENTS

We would like to express our appreciation to Drs Keiichi Akahane and Silvan Zenklusen for their useful advice and discussion.

REFERENCES

1. Britton KR, Starkschall G, Tucker SL *et al*. Assessment of gross tumor volume regression and motion changes during radiotherapy for non-small-cell lung cancer as measured by four-dimensional computed tomography. *Int J Radiat Oncol Biol Phys* 2007;**68**:1036–46.
2. Mori S, Kanematsu N, Asakura H *et al*. Four-dimensional lung treatment planning in layer-stacking carbon ion beam treatment: comparison of layer-stacking and conventional ungated/gated irradiation. *Int J Radiat Oncol Biol Phys* 2011;**80**:597–607.
3. Mori S, Ko S, Ishii T *et al*. Effective doses in four-dimensional computed tomography for lung radiotherapy planning. *Med Dosim* 2009;**34**:87–90.
4. Low DA, Nystrom M, Kalinin E *et al*. A method for the reconstruction of four-dimensional synchronized CT scans acquired during free breathing. *Med Phys* 2003;**30**:1254–63.
5. DeMarco JJ, McNitt-Gray MF, Cagnon CH *et al*. Evaluation of patient dose using a virtual CT scanner: Applications to 4DCT simulation and Kilovoltage cone-beam imaging. *J Phys Conf Ser* 2008;**102**:012006.
6. Keall PJ, Starkschall G, Shukla H *et al*. Acquiring 4D thoracic CT scans using a multislice helical method. *Phys Med Biol* 2004;**49**:2053–67.
7. Nishizawa K, Mori S, Ohno M *et al*. Patient dose estimation for multi-detector-row CT examinations. *Radiat Prot Dosimetry* 2008;**128**:98–105.
8. Hiraoka T, Kawashima K, Hoshino K *et al*. Development of bone substitute materials. *Radiotherapy System Research Supplement* 1987;**4**:93–6.
9. Hirooka T, Irifune T, Kawashima K *et al*. Trial manufacture of inhomogeneous phantom. *Radiotherapy System Research Supplement* 1988;**5**:34–7.
10. ICRP. The 1990 Recommendations of the International Commission on Radiological Protection. ICRP Publication 60. Ann ICRP *1991*;**21**:1–201.
11. ICRP. The 2007 Recommendations of the International Commission on Radiological Protection. ICRP Publication 103. *Ann ICRP* 2007;**37**:1–332.
12. Fujii K, Aoyama T, Koyama S *et al*. Comparative evaluation of organ and effective doses for paediatric patients with those for adults in chest and abdominal CT examinations. *Br J Radiol* 2007;**80**:657–67.
13. ICRP. Age-dependent doses to members of the public from intake of radionuclides: Part 2. Ingestion dose coefficients. A report of a Task Group of Committee 2 of the International Commission on Radiological Protection. ICRP Publication 67. *Ann ICRP* 1993;**23**:1–167.
14. McParland BJ. *Nuclear Medicine Radiation Dosimetry: Advanced Theoretical Principles*. Dordrecht, Netherlands: Springer, 2010.
15. Nishizawa K, Maruyama T, Takayama M *et al*. Determinations of organ doses and effective dose equivalents from computed tomographic examination. *Br J Radiol* 1991;**64**:20–8.
16. Taguchi K. Temporal resolution and the evaluation of candidate algorithms for four-dimensional CT. *Med Phys* 2003; **30**:640–50.
17. Mori S, Nishizawa K, Kondo C *et al*. Effective doses in subjects undergoing computed tomography cardiac imaging with the 256-multislice CT scanner. *Eur J Radiol* 2008;**65**:442–8.
18. McCollough CH, Primak AN, Saba O *et al*. Dose performance of a 64-channel dual-source CT scanner. *Radiology* 2007;**243**:775–84.

19. Hunold P, Vogt FM, Schmermund A *et al*. Radiation exposure during cardiac CT: effective doses at multi-detector row CT and electron-beam CT. *Radiology* 2003;**226**:145–52.
20. Kachelriess M, Knaup M, Kalender WA. Extended parallel backprojection for standard three-dimensional and phase-correlated four-dimensional axial and spiral cone-beam CT with arbitrary pitch, arbitrary cone-angle, and 100% dose usage. *Med Phys* 2004;**31**:1623–41.
21. Mitsumori LM, Shuman WP, Busey JM *et al*. Adaptive statistical iterative reconstruction versus filtered back projection in the same patient: 64 channel liver CT image quality and patient radiation dose. *Eur Radiol* 2012;**22**:138–43.
22. NCCN (National Comprehensive Cancer Network). NCCN clinical practice guidelines in oncology: Non-Small Cell Lung Cancer. v.2.2013:Available from: http://www.nccn.org/professionals/physician_gls/pdf/nscl.pdf. (1 January, 2012, date last accessed)